Published OnlineFirst on September 21, 2010 as 10.1158/1078-0432.CCR-10-1206

Clinical Cancer Research

Imaging, Diagnosis, Prognosis

See commentary p. 4685

Hypoxia in Models of Lung Cancer: Implications for Targeted Therapeutics

Edward E. Graves[1], Marta Vilalta[1], Ivana K. Cecic[1], Janine T. Erler[1], Phuoc T. Tran[1], Dean Felsher[2], Leanne Sayles[3], Alejandro Sweet-Cordero[3], Quynh-Thu Le[1], and Amato J. Giaccia[1]

Abstract

Purpose: To efficiently translate experimental methods from bench to bedside, it is imperative that laboratory models of cancer mimic human disease as closely as possible. In this study, we sought to compare patterns of hypoxia in several standard and emerging mouse models of lung cancer to establish the appropriateness of each for evaluating the role of oxygen in lung cancer progression and therapeutic response.

Experimental Design: Subcutaneous and orthotopic human A549 lung carcinomas growing in nude mice as well as spontaneous *K-ras* or *Myc*-induced lung tumors grown *in situ* or subcutaneously were studied using fluorodeoxyglucose and fluoroazomycin arabinoside positron emission tomography, and postmortem by immunohistochemical observation of the hypoxia marker pimonidazole. The response of these models to the hypoxia-activated cytotoxin PR-104 was also quantified by the formation of γH2AX foci *in vitro* and *in vivo*. Finally, our findings were compared with oxygen electrode measurements of human lung cancers.

Results: Minimal fluoroazomycin arabinoside and pimonidazole accumulation was seen in tumors growing within the lungs, whereas subcutaneous tumors showed substantial trapping of both hypoxia probes. These observations correlated with the response of these tumors to PR-104, and with the reduced incidence of hypoxia in human lung cancers relative to other solid tumor types.

Conclusions: These findings suggest that *in situ* models of lung cancer in mice may be more reflective of the human disease, and encourage judicious selection of preclinical tumor models for the study of hypoxia imaging and antihypoxic cell therapies. *Clin Cancer Res; 16(19); 4843–52. ©2010 AACR.*

The role of oxygen in the response of tumors to treatment has been noted since the experiments of Thomlinson (1) and Gray (2). Hypoxia is a common phenomenon in human tumors, with most tumors possessing lower oxygenation than their corresponding tissue of origin (3). An aggressive phenotype has been associated with hypoxic tumors, encompassing both the well-studied resistance of poorly oxygenated cancers to radiotherapy and chemotherapy as well as a propensity for hypoxic tumors to exhibit increased potential for invasion, growth, and metastasis (4–11). Given the enormous relevance of hypoxia and the hypoxic tumor phenotype to the clinical management of cancer, much attention has been given to the development of treatments that target hypoxic tumor cells. With the emergence of noninvasive methods for imaging hypoxia, the use of oxygen status as a factor in tumor staging, treatment selection, and radiotherapy planning has been advanced (3, 12). In recent years, several hypoxia-selective chemotherapeutics that specifically target and kill hypoxic cells have been investigated, including tirapazamine (13) and PR-104 (14). These agents offer the possibility of specifically targeting and overcoming hypoxia and the therapeutic resistance associated with it.

To establish and optimize hypoxia-targeted therapies, it is necessary to study the application of these treatments in preclinical models of cancer. The most common experimental tumor model is one in which human tumor cells are grown subcutaneously in an immune-compromised mouse. This is a convenient model in that tumor growth can be observed visually, and the tumor is accessible for tissue sampling or treatment. More sophisticated orthotopic experimental tumor models in which neoplastic cells are implanted and grown within the organ from which they were derived have also existed for many years (15). These models have been shown to exhibit metastatic behavior and therapeutic responses that more closely follow those encountered with the corresponding human cancers in the clinic (16–21). Vascular growth patterns within both primary orthotopic tumors and their

Authors' Affiliations: Departments of [1]Radiation Oncology, [2]Medicine, and [3]Pediatrics, Molecular Imaging Program at Stanford, Stanford University, Stanford, California

Corresponding Author: Edward E. Graves, Department of Radiation Oncology, Stanford University, 875 Blake Wilbur Drive, Room G-202, Stanford, CA 94305-5847. Phone: 650-723-5591; Fax: 650-498-4015; E-mail: egraves@stanford.edu.

doi: 10.1158/1078-0432.CCR-10-1206

Translational Relevance

The focus of this research is to establish the relevance of preclinical mouse models of lung cancer to the corresponding human disease. It is observed through our experiments that the most common mouse tumor model, the subcutaneous xenograft, may significantly overestimate the degree of hypoxia in these tumors. This calls into question the appropriateness of conclusions from tumor biology and therapy studies employing this model when translated into clinical practice. The findings of this research will influence model selection for future laboratory studies of lung tumor biology, improving the link between preclinical research and clinical practice.

metastases have been noted to differ significantly from those of primary and metastatic tumors of the same genotype grown subcutaneously (22). Although tumor-associated vasculature is strongly influenced by the tumor itself, this observed difference between orthotopic and subcutaneous tumors suggests that orthotopically grown tumors may be more clinically relevant models of cancer in which to study the biology of this disease and evaluate novel therapeutic strategies. At present, humane strategies for orthotopic implantation and growth of tumors in mice exist for a number of cancer types, including brain, colon, head and neck, lung, ovarian, pancreas, and prostate. When grown in immune-compromised mice, these cancer modeling techniques permit the growth of human tumors within a laboratory animal. However, the xenograft nature of these models may interfere with tumor-stroma interactions and distinguish these models from the corresponding human disease. Therefore, cancer biologists have used transgenic mouse technology to generate rodent strains that spontaneously develop tumors to more effectively recapitulate the natural history of tumorigenesis and tumor progression. These include the transgenic adenocarcinoma mouse prostate model (23), and recently, several tissue-specific oncogene-induced spontaneous cancers (24, 25).

Although it is generally accepted that orthotopic and spontaneous models of cancer provide experimental systems that are more relevant to human disease, subcutaneous tumor models remain the workhorse of cancer biology investigations. We therefore sought to investigate potential discrepancies in the tumor microenvironment between a number of preclinical models of lung cancer, to assess how model selection might affect the results of studies of tumor biology and therapeutic response. We employed both established and emerging methods of assessing hypoxia in this study, and compared the preclinical findings with measurements acquired from human lung tumors. Our findings encourage both judicious selection of models for preclinical studies of lung cancer, as well as careful consideration and further study of the role of hypoxia in lung tumor progression and therapeutic response in the clinic.

Materials and Methods

Animal models

All animal experiments were done according to a protocol approved by the Institutional Animal Care and Use Committee. Human A549 lung carcinoma cells bearing an activating *K-ras* mutation (26) were stably transfected with firefly luciferase and grown either subcutaneously or orthotopically in male *nu/nu* nude mice. To produce subcutaneous tumors, 10^6 tumor cells were injected beneath the skin on each shoulder of a mouse. To implant tumor cells in an orthotopic location, the mice were anesthetized and an incision was made on the abdomen just below the ribcage. Tumor cells were then injected into the base of the lung via a needle passed through the diaphragm. The injection site was then sealed with Matrigel and the incision sutured, after which the mice were allowed to recover under supplemental analgesia. Tumor growth was monitored by weekly bioluminescence imaging studies acquired using an IVIS 200 imaging system (Caliper Biosciences).

Expression of the *K-ras* oncogene in cells of the lung of male *nu/nu* nude mice was induced using a nasally delivered adeno-Cre construct delivered nasally to the lungs of transgenic mice bearing a *Lox-Stop-Lox-K-ras* gene as described previously (24), resulting in focal *K-ras*–positive lung lesions within 4 to 6 weeks of infection. Lung-specific expression of a tetracycline-inducible *Myc* oncogene vector and subsequent tumor induction was achieved in nude mice as described by Tran et al. (27). For both of these models, tumor formation in the lung was monitored by weekly X-ray computed tomography (CT) scans using an eXplore Locus RS120 micro-CT scanner (GE Health Care). Tumors generated in a subset of *K-ras*– and *Myc*-induced mice were harvested and used to produce cell lines *in vitro*.

Micro-positron emission tomography imaging

Fluoroazomycin arabinoside (FAZA) was synthesized with a TracerLab FX-FN automated nucleophilic synthesis system (GE Health Care) using [^{18}F]fluoride produced on a PETtrace cyclotron (GE Health Care), following the procedure of Reischl et al. (28) implemented on an FX-FN automated radiotracer synthesis module (GE Health Care). Fluorodeoxyglucose (FDG) was produced in a dedicated synthesis unit. Beginning 8 weeks after tumor implantation, animals underwent FDG and FAZA micro-positron emission tomography (PET) examinations on subsequent days every 2 weeks. Each subject received an i.v. injection of ~200 mCi in 100 mL of radiotracer before undergoing micro-PET imaging on a Rodent R4 scanner (Concorde Microsystems). Circulation times between radiotracer injection and imaging were 1 hour for FDG and 3 hours for FAZA. During imaging, coincidence events

were collected for 10 minutes and reconstructed into three-dimensional image data using an ordered subsets expectation maximization algorithm. Data was quantified in units of percentage of injected dose per gram (% ID/g) and displayed and analyzed using region-of-interest methods within the RT_Image software package (29). Regions-of-interest were drawn manually over visible tumor areas and over the entire lung volume, and the mean and SD of pixels within these regions were calculated. In addition, regions-of-interest were drawn for each mouse over the normal skeletal muscle to quantify background uptake. Image intensities were considered both in units of percentage of injected dose per gram and the ratio of target to the measured background tissue uptake (T/B).

Immunohistochemistry

After micro-PET imaging, the hypoxia marker pimonidazole (Chemicon International, Inc.) was given i.v. to mice at a dose of 100 mg/kg body weight. One hour after injection, the mice were humanely euthanized and the subcutaneous tumor or the lungs were excised, fixed with formalin, embedded in paraffin, and cut into 4-μm sections. After mounting on slides, these sections were stained for pimonidazole adducts using an antipimonidazole antibody as described previously (30).

Hypoxia-targeted chemotherapy

To assess the efficacy of a hypoxia-directed therapy on models of lung cancer, tumor cells grown *in vitro* and *in vivo* were treated with the dinitrobenzamide mustard PR-104, a drug that has been previously shown to selectively kill cells under hypoxic conditions (14). Cells harvested from *Myc*-induced murine lung cancers and from the Kras-induced murine lung cancer model as well as the human lung cancer cell line A549 were grown *in vitro*. Cells were plated in two-well culture slides and treated the following day with 100 μmol/L of PR-104 (Proacta, Inc.) for 4 hours under different oxygen concentrations (0.5%, 2%, and 21%). After the treatment period, cells were rinsed with PBS and grown for 3 hours in standard conditions, then rinsed with PBS and fixed with 4% formalin for 15 minutes. Immunohistochemistry was performed by incubating with an anti-phosphorylated histone γH2AX (Ser^{139}) mouse monoclonal antibody (Millipore) at a 1:700 dilution for 2 hours at room temperature, followed by incubation with a Texas red horse anti-mouse IgG antibody (Vector Laboratories) at a 1:80 dilution for 1 hour. Cell nuclei were stained with 4′,6-diamidino-2-phenylindole (DAPI) solution (Millipore).

In addition, mice with *K-ras*– and *Myc*-inducible lung tumors as well as mice bearing subcutaneous A549 tumors were treated with 1.8 mmol/kg body weight of PR-104 delivered i.p. Eighteen hours after a single PR-104 treatment, mice were euthanized through CO_2 inhalation. The lungs of mice with tumors *in situ* were excised and inflated before fixing with 10% formalin for 24 hours. Lungs were then washed with PBS and embedded in paraffin. Subcutaneous A549 tumors were excised and fixed with 10% formalin for 24 hours before rinsing in PBS and embedding in paraffin. Mice with subcutaneous A549 tumors sacrificed 1 hour after treatment with a 10 Gy dose of ionizing radiation were analyzed as a positive control for γH2AX induction *in vivo*. Microtome sections were generated and mounted on silanized slides. Immunohistochemistry was performed after antigen retrieval with 10 mmol/L of citric acid (pH = 6) by incubating with the anti-phosphorylated histone γH2AX (Ser^{139}) at 1:700 for 12 hours at 4°C followed by Texas red horse anti-mouse IgG (Vector Laboratories) at a 1:80 dilution for 1 hour at room temperature. As above, staining for DAPI was used to visualize cell nuclei.

To quantify the formation of γH2AX foci on microscopy data, RT_Image was used to delineate cell nuclei based on the DAPI image, and then to compute the sum of all pixel intensities in the γH2AX image within the DAPI-positive areas. The average total γH2AX signal per cell was then computed and normalized to a measure of the background intensity for each microscopy image and compared between samples.

Human tumor pO_2 measurements

Patients with histologically verified lung cancer were studied using an oxygen electrode. At the time of surgical resection, a computerized Eppendorf pO_2 histograph (Sigma) was used to measure oxygen tensions within the tumor and adjacent normal tissue as described previously (31). The 60 to 100 individual oxygen measurements collected from each patient were analyzed by computing the median pO_2 as well as the fraction of measurements <2.5 mm Hg (HF2.5) and <10 mm Hg (HF10).

Results

In vivo imaging

A total of 25 tumor-bearing mice were studied: 5 with subcutaneous A549 tumors, 9 with orthotopically implanted A549 lung carcinomas, 5 with spontaneous *Myc*-induced lung lesions, and 6 with spontaneous *K-ras*–induced lung lesions. The subcutaneous A549 lesions grew to ~0.5 cc volumes within 6 weeks, whereas the orthotopically implanted A549 mice were monitored with bioluminescence imaging up to 30 weeks postimplantation, at which time the mice exhibited tumor-related morbidity and were humanely euthanized. The *K-ras* and *Myc*-induced tumors were followed with weekly micro-CT imaging over a period of 10 and 30 weeks, respectively, consistent with other studies employing these models (24, 27). PET imaging examinations were performed using well-established, late stage tumors of 5 to 7 mm diameter at 6 weeks (subcutaneous A549), 8 weeks (orthotopic A549), 8 weeks (spontaneous *K-ras*), and 30 weeks (spontaneous *Myc*) post-initiation.

Representative results of micro-CT, FDG micro-PET, FAZA micro-PET, and pimonidazole immunohistochemistry studies performed for terminal lung cancer–bearing mice are shown in Fig. 1A. A conspicuous subcutaneous

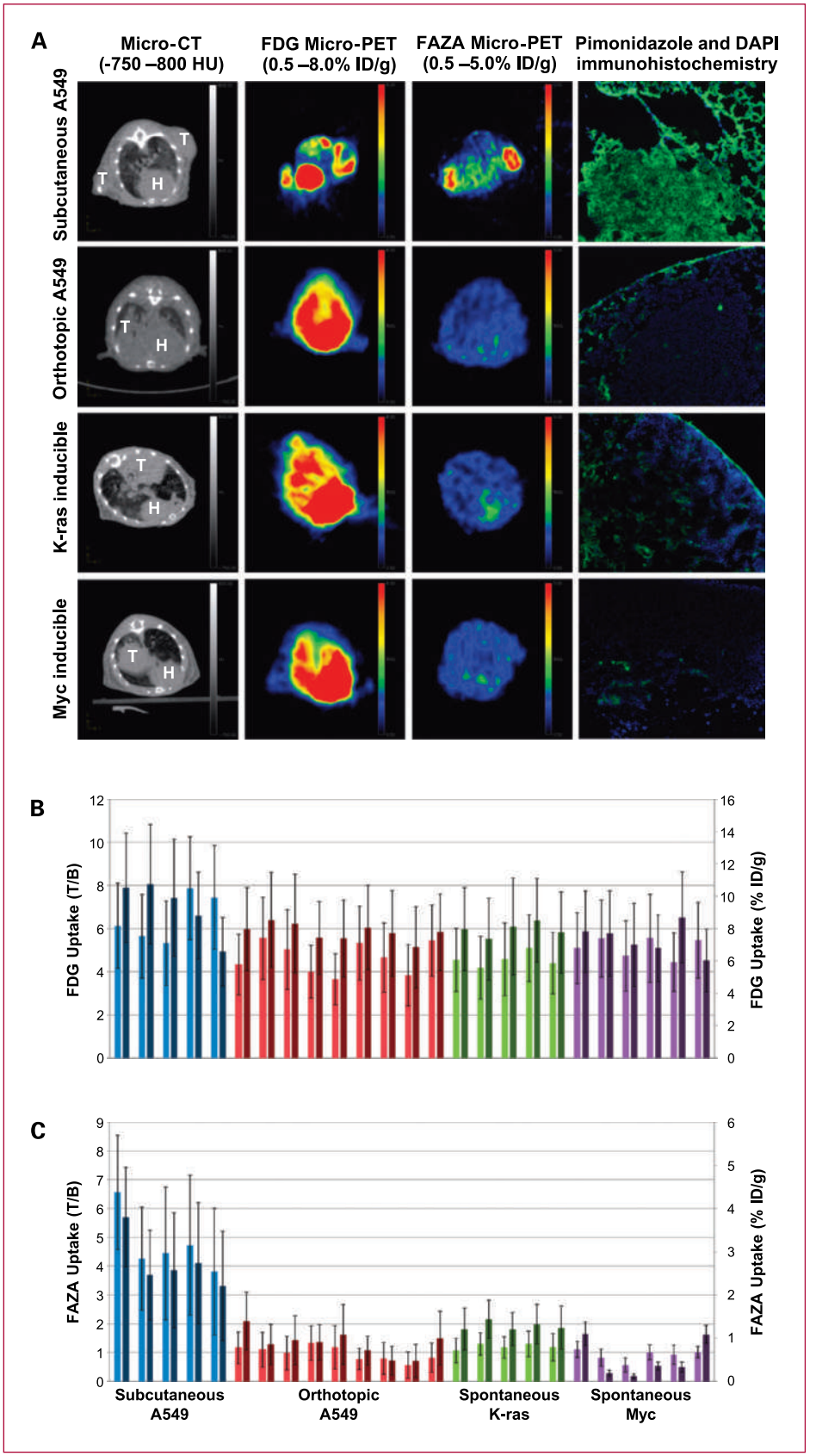

Fig. 1. *In vivo* imaging and *ex vivo* immunohistochemistry of murine models of lung cancer. A, results obtained from bilateral subcutaneous A549 xenograft tumors (top row), orthotopically implanted A549 xenograft tumors (second row), spontaneous *K-ras*–induced lung tumors (third row), and spontaneous *Myc*-induced lung tumors (bottom row). The data collected from each subject included micro-CT (left column), FDG micro-PET (second column), FAZA micro-PET (third column), and pimonidazole (green) and DAPI (blue) immunohistochemistry (right column). Displayed intensity ranges for *in vivo* imaging are given (top). Relevant features are labeled on the CT images, including tumor (T) and heart (H). B and C, mean FDG and FAZA uptake observed in micro-PET studies of murine models of lung cancer. The light-colored bars are quantified in units of tumor/background ratio (T/B, left vertical axis), whereas the dark-colored bars are in units of percentage injected dose per gram of tissue (% ID/g, right vertical axis). Blue, subcutaneous A549 xenograft tumors; red, orthotopic A549 xenograft tumors; green, spontaneous *K-ras*–induced lung tumors; purple, spontaneous *Myc*-induced lung tumors. The measurements reported for the subcutaneous tumors indicate the mean and SD over a region-of-interest defined over the tumor, whereas the measurements for the orthotopic and spontaneous tumors are the mean and SD over a region-of-interest encompassing the lungs and excluding the heart.

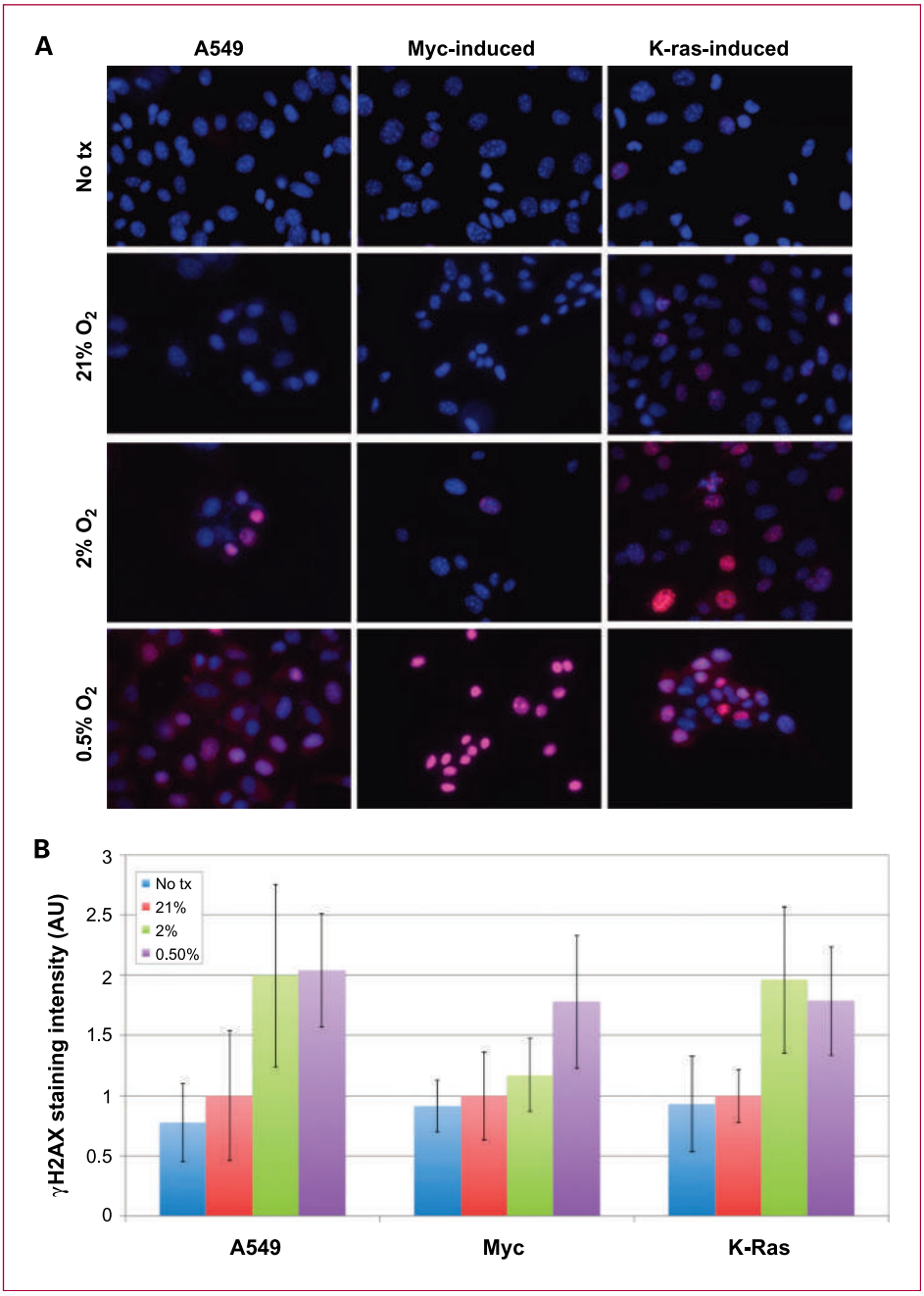

Fig. 2. Response of lung tumor cell lines to PR-104 treatment *in vitro*. A, γH2AX (red) and DAPI (blue) immunohistochemistry of human A549, murine *Myc*-induced lung carcinoma, and murine *K-ras*–induced lung carcinoma cells treated with 100 μmol/L of PR-104 for 4 h in 21%, 2%, or 0.5% O_2. Untreated cells of each type are shown as a control. B, quantitated average total γH2AX signal per cell for each treatment group and cell type. Blue, untreated cells; red, cells treated at 21% O_2; green, cells treated at 2% O_2; purple, cells treated at 0.5% O_2. All measurements for a cell type are normalized to the average total γH2AX signal per cell for that cell type treated at 21% O_2.

mass is apparent for the subcutaneous A549 tumor-bearing mouse on the micro-CT scan, which traps both FDG and FAZA as seen on the micro-PET images. A widespread hyperintensity is noticeable within the lungs of the orthotopic A549 tumor-bearing mouse on the micro-CT image. Although the heart exhibits intense FDG accumulation as seen in the micro-PET examination, significant uptake of FDG is also noted in both lobes of the lung. However, no detectable FAZA uptake above background is noted in the vicinity of the lungs, except for a small hyperintensity coincident with the heart. In mice with lung-specific activation of the *K-ras* and *Myc* oncogenes, one or more large neoplastic masses were evident on the micro-CT scan. These lesions display intense accumulation of FDG that can be differentiated from cardiac uptake, but as in the orthotopic A549 mice, no elevated trapping of FAZA within the volume of the lungs is evident. Pimonidazole staining of these tumor specimens following animal sacrifice and tissue harvesting is in agreement with the FAZA findings, showing minimal labeling of the orthotopic and spontaneous tumors while binding strongly to the subcutaneous lesion. Quantitative analysis of the complete set of

micro-PET data collected from this subject population is shown in Fig. 1B and C.

Hypoxia-targeted chemotherapy

Figure 2A shows representative γH2AX (red) and DAPI (blue) immunohistochemistry results from human A549 cells, two *Myc*-induced cell lines (B7347 and B7348), and two *K-ras*–induced cell lines (LKR10 and LKR13) treated with PR-104 *in vitro* under several oxygen conditions. In general, DNA damage as indicated by γH2AX staining increases with decreasing oxygenation in all three cell types. These observations are quantified in Fig. 2B, in which the average normalized γH2AX staining per cell is plotted for each cell type and oxygen level. All three lines exhibit statistically significant increases in γH2AX staining between 21% and 0.5% O_2 ($P < 0.05$). Having observed the sensitivity of each of these cell types to hypoxia-mediated PR-104–induced DNA damage, the response of these tumors to PR-104 treatment *in vivo* was then measured. Figure 3 shows representative immunohistochemical slides collected from these tumors and quantification of the data collected. The dramatic increase in γH2AX staining in PR-104–treated A549 tumors is statistically significant when compared with samples from untreated A549 tumors ($P < 0.0001$) as well as to untreated and PR-104–treated spontaneous *Myc*- and *K-ras*–induced lung tumors ($P < 0.0001$). Neither of the spontaneous tumor models exhibited a significant increase in γH2AX signal after treatment with PR-104, compared with untreated controls.

Human tumor pO_2 measurements

A total of 24 patients with primary non–small cell lung cancer comprised the clinical patient sample. Figure 4A shows the distribution of median tumor pO_2 for the lung cancers. The median pO_2 for this group of lung cancers was 13.5 mm Hg, with a range of 0.7 to 45.6 mm Hg. A previous multi-institutional study suggested that the hypoxic fraction HF2.5 (percentage of measurements <2.5 mm Hg) was the most predictive factor for survival in head and neck cancer, with a threshold HF2.5 of 20% (32). Therefore, we also evaluated the HF2.5 for this lung tumor sample, as well as the fraction of patients with HF2.5 ≥20%. In addition, we calculated HF10 and HF10 ≥20% to estimate how many human lung cancers would

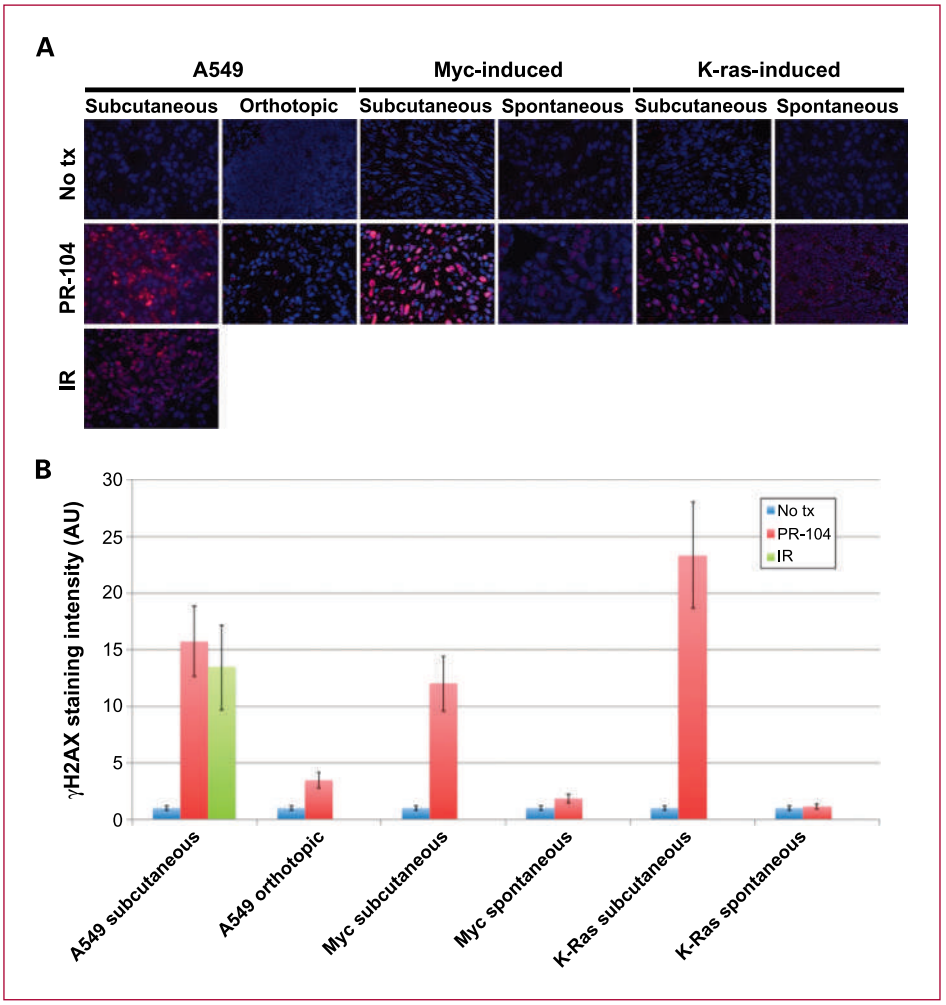

Fig. 3. Response of murine lung tumor models to PR-104 treatment *in vivo*. A, γH2AX (red) and DAPI (blue) immunohistochemistry of subcutaneous and orthotopic A549 tumor xenografts, spontaneous and subcutaneous *Myc*-induced lung carcinomas, and spontaneous and subcutaneous *K-ras*–induced lung carcinomas treated with a single i.p. dose of 1.8 mmol/kg of PR-104 for 18 h prior to tissue harvesting. Data collected from subcutaneous A549 tumors treated with 10 Gy of ionizing radiation are shown as a positive control. B, quantitated average total γH2AX signal per cell for each treatment group and tumor type. Blue, untreated tumors; red, PR-104–treated tumors; green, IR-treated tumors. All measurements for a tumor type are normalized to the average total γH2AX signal per cell for that tumor observed without treatment.

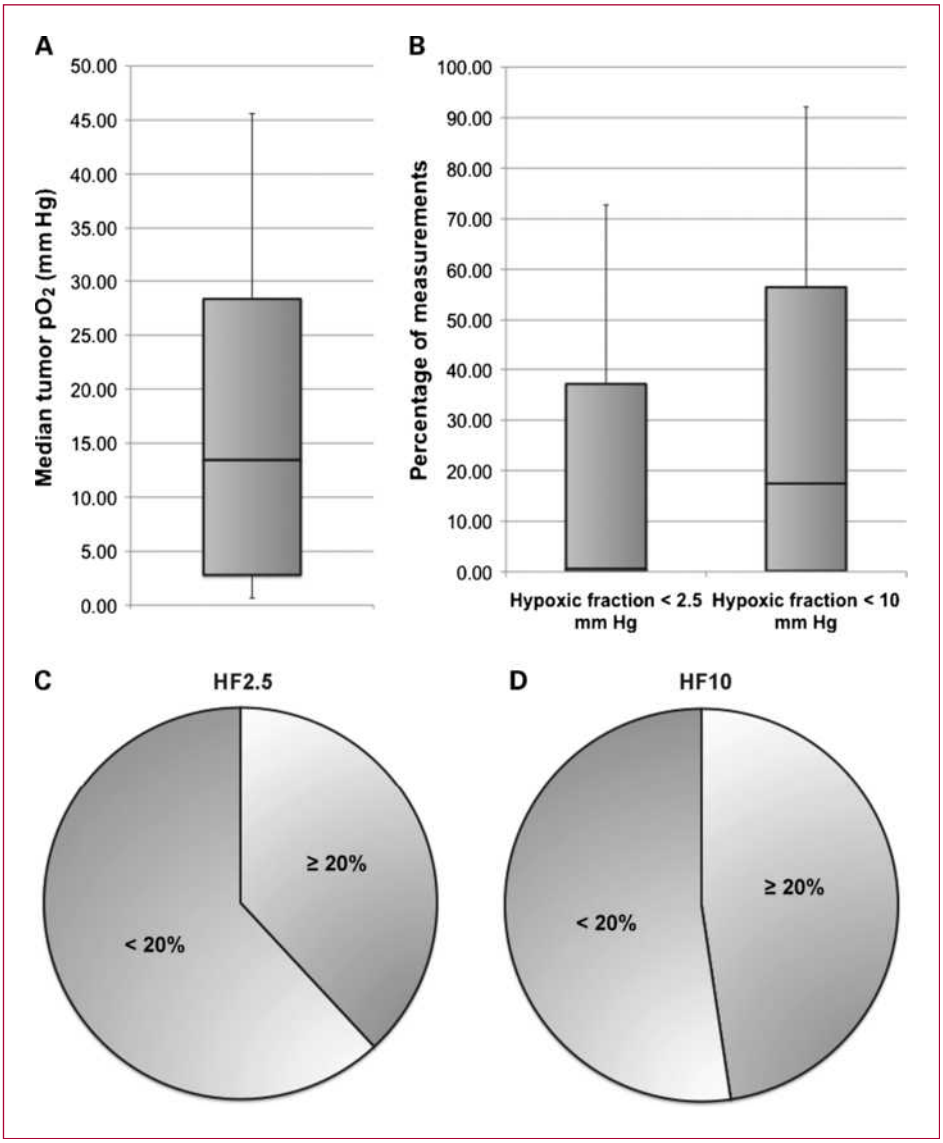

Fig. 4. *In vivo* Eppendorf electrode measurements of oxygenation of human lung cancers. A, box and whisker plot showing the distribution of median tumor pO_2 measurements for 21 non–small cell lung cancer patients. B, box and whisker plot showing the distribution of the percentage of oxygen measurements <2.5 mm Hg (HF2.5) and <10 mm Hg (HF10) for this patient sample. C, pie chart demonstrating the proportion of lung cancer patients with HF2.5 above and below a threshold value of 20%. D, pie chart demonstrating the proportion of lung cancer patients with HF10 above and below a threshold value of 20%.

accumulate in the hypoxia probes pimonidazole and FAZA, using 10 mm Hg as an approximate threshold for binding of these agents (33, 34). These data are presented in Fig. 4B and C. The median HF2.5 and HF10 values for this patient sample were 0.6% and 17.5%, respectively; 38.1% of patients exhibited an HF2.5 of ≥20%, whereas 47.6% of patients displayed an HF10 of ≥20%.

Discussion

Although cell culture systems allow rigorous investigation of the molecular biology of cancer, they lack components such as vasculature and immune responses that complicate the extrapolation of results to the *in vivo* situation. Murine tumor models allow the evaluation of cancer biology within an intact, living organism. The simplest mouse models of neoplasm involve the introduction of human cancer cells beneath the skin of immune-compromised mice. This technique facilitates the development of subcutaneous tumors genetically identical to those found in humans. However, it is generally acknowledged that the vasculature, and correspondingly, the perfusion and oxygen status of these lesions may differ from human disease because of the immediate tissue environment of the subcutaneous space (21). Although potentially more relevant orthotopic and spontaneous models of cancer have been developed (16, 18, 19), subcutaneous tumor models remain the workhorse of preclinical cancer biology research.

The goal of this study was to investigate the significance of model type in preclinical studies of hypoxia in lung cancer. The incidence of hypoxia was assessed in subcutaneous and orthotopic xenograft models of human cancer as well as in spontaneous oncogene-induced murine lung tumors. Although all tumors studied exhibited elevated

metabolism and glycolytic activity as observed with FDG-PET imaging, only the subcutaneous tumors showed significant hypoxia as seen in both FAZA PET and pimonidazole immunohistochemical assays. Neither the orthotopic xenografts nor the spontaneous murine tumors exhibited significant uptake of FAZA or pimonidazole, suggesting that at both the microscopic and macroscopic levels, these lesions are relatively well-oxygenated. The orthotopically implanted A549 tumors grew as diffuse microscopic clusters of cells that eventually overtook the entire lung, as seen in the micro-CT image in Fig. 1. This may account for the lack of hypoxia in this model because small lesions interspersed within normal lung parenchyma would not be expected to exhibit poor oxygenation. However, both the *K-ras*– and *Myc*-induced spontaneous tumors grew as focal masses to large sizes (1 cc), similar to human lung cancer, and neither displayed measurable hypoxia either by macroscopic imaging or microscopic immunohistochemistry assays. The microscopic cause of this discrepancy in oxygenation between the tumor models was not investigated, but is presumed to be due to differences in the vascular networks formed by these tumors. Interestingly, these measures of tumoral hypoxia correlated with response to PR-104 treatment for all tumor types studied. Although each tumor cell type responded to PR-104 *in vitro* under hypoxic conditions (Fig. 2), only the subcutaneously grown A549 tumor xenograft exhibited a response to PR-104 *in vivo* (Fig. 3), consistent with the observation of extensive hypoxia in this model.

The implications of these observations for preclinical studies of tumor biology and therapeutics are significant. Clearly, the findings from preclinical studies of the efficacy of hypoxia-directed therapies such as tirapazamine (35), PR-104 (14), and HIF-1 inhibitors (36) will be inextricably tied to the models in which these investigations were conducted. The observations presented here show that such therapies will be preferentially effective in subcutaneous tumor models that have poor oxygenation, and less effective in orthotopic and spontaneous disease models. The appropriateness of each model type for these therapeutic investigations is dictated on which model is most reflective of human lung cancer. The oxygenation of human lung cancers measured here using an Eppendorf electrode is larger than comparable measures of head and neck cancer acquired by our group, in terms of median pO_2 (lung, 13.5 mm Hg; head and neck, 11.4 mm Hg) and HF2.5 (lung, 0.6%; head and neck, 12.4%), although these differences are not statistically significant. This is consistent with other reports that the median oxygenation of lung tumors is generally greater than other solid tumor types (37) and is in the transition oxygen range between strong and weak cellular accumulation of 2-nitroimidazole hypoxia probes such as FAZA (33, 34). It is also interesting to note that initial studies of orthotopic and subcutaneous models of head and neck cancer conducted by our group have shown the incidence of hypoxia in both model types, an observation which supports the hypothesis that these cancers have lower oxygenation *in situ* than lung tumors. A recent preliminary study of hypofractionated radiotherapy for lung tumors reported excellent 3-year primary and locoregional control rates (97.6% and 87.2%, respectively; ref. 38). Whereas the biologically effective dose delivered in this regimen is very large and might explain the response rates, it is interesting to note that according to classical radiobiology, one would expect hypoxic tumors to respond poorly to such a hypofractionated radiotherapy course.

In vivo imaging of tumoral hypoxia is a technique that has been developed over the last 20 years (39). A number of hypoxia-specific PET radiotracers, including ^{18}F-fluoromisonidazole (FMISO), FAZA, ^{64}Cu-ATSM, and EF5, have been applied towards this end and many are now undergoing clinical evaluation. The ability of FAZA to label regions of hypoxic tissue has been evaluated in several preclinical studies (40, 41), with FAZA uptake correlating with immunohistochemical electrode measures of hypoxia. Investigations of hypoxia in human lung cancer using nuclear medicine techniques have shown ^{60}Cu-ATSM tumor/muscle ratios of 1.2 to 4.8 (mean, 2.3; ref. 42), ^{18}FMISO tumor/normal ratios of 1.17 to 3.76 (mean, 1.92; ref. 43), and ^{99m}Tc-HL91 tumor/normal ratios of 1.13 to 1.90 (mean, 1.57; ref. 44). In our clinical lung tumor cohort, we observed 47.6% of patients with an HF10 ≥20%. Using 10 mm Hg as a threshold for hypoxia probe binding and 20% as the minimum hypoxic fraction of a tumor required to be visible on a hypoxia nuclear medicine scan, this suggests that roughly half of these patients would give a positive imaging signal. Although this is a coarse estimate, it corresponds well to the imaging studies cited above. Variations in lung cancer oxygenation are evident from imaging studies, however, it is informative to note that on average oxygen levels of lung tumors are higher than those of other solid tumors. This suggests that the absence of hypoxia in the orthotopic and spontaneous tumor models observed here using FAZA PET may be reflective of the reduced incidence of hypoxia in this tumor type when growing *in situ*.

Although current data supports the conclusion that macroscopic PET imaging could differentiate between grossly hypoxic and well-oxygenated tumors, what remains unclear is the dynamic range of this imaging modality. The majority of studies of the utility of hypoxia PET in predicting response to therapy have retrospectively stratified the sample populations into "hypoxic" and "normoxic" groups on the basis of the mean or median uptake seen on a hypoxia PET scan (35, 42), which in practice results in a threshold on the order of a T/B ratio of 2. The group at the University of Washington studying FMISO have alternately devised a strategy for computing the fractional hypoxic volume of a tumor, using a threshold tumor/blood ratio of 1.2 (45). It is interesting to note that although recent radiobiological research has stressed the significance of the full spectrum of tissue oxygenation states from fully anoxic to normoxic (46), in particular the potential importance of intermediately hypoxic cells in dictating hypoxic tumor therapeutic resistance, efforts

to apply hypoxia PET as a clinical prognostic variable have generally characterized tumors through a binary, "hypoxic," or "normoxic" strategy. Although some preliminary positive retrospective studies employing such methods have yielded promising results (47), it remains to be seen whether this simplified assessment of the tumor microenvironment will prove effective in large-scale clinical trials. Continued development of PET radiotracers with improved sensitivity and specificity for hypoxic tissue will undoubtedly increase enthusiasm for widespread adoption of hypoxia imaging as a staging examination.

Disclosure of Potential Conflicts of Interest

No potential conflicts of interest were disclosed.

Acknowledgments

We gratefully acknowledge the assistance of Drs. Frederick Chin, David Dick, and Tim Doyle for assistance with animal models, radiotracer production, and micro-PET imaging.

Grant Support

Charles Henry Leach II Foundation, Lerner Family Foundation, NIH R01 CA131199, NIH P01 CA067166.

The costs of publication of this article were defrayed in part by the payment of page charges. This article must therefore be hereby marked *advertisement* in accordance with 18 U.S.C. Section 1734 solely to indicate this fact.

Received 05/12/2010; revised 06/30/2010; accepted 07/13/2010; published OnlineFirst 09/21/2010.

References

1. Thomlinson RH, Gray LH. The histological structure of some human lung cancers and the possible implications for radiotherapy. Br J Cancer 1955;9:539–49.
2. Gray LH, Conger AD, Ebert M, Hornsey S, Scott OCA. The concentration of oxygen dissolved in tissues at the time of irradiation as a factor in radiotherapy. Br J Radiol 1953;26:638–48.
3. Höckel M, Vaupel P. Tumor hypoxia: definitions and current clinical, biologic, and molecular aspects. J Natl Cancer Inst 2001;93:266–76.
4. Young SD, Marshall RS, Hill RP. Hypoxia induces DNA overreplication and enhances metastatic potential of murine tumor cells. Proc Natl Acad Sci U S A 1988;85:9533–7.
5. Brizel DM, Scully SP, Harrelson JM, et al. Tumor oxygenation predicts for the likelihood of distant metastases in human soft tissue sarcoma. Cancer Res 1996;56:941–3.
6. Höckel M, Schlenger K, Aral B, Mitze M, Schaffer U, Vaupel P. Association between tumor hypoxia and malignant progression in advanced cancer of the uterine cervix. Cancer Res 1996;56:4509–915.
7. Brizel DM, Sibley GS, Prosnitz LR, Scher RL, Dewhirst MW. Tumor hypoxia adversely affects the prognosis of carcinoma of the head and neck. Int J Radiat Oncol Biol Phys 1997;38:285–9.
8. Cuvier C, Jang A, Hill RP. Exposure to hypoxia, glucose starvation and acidosis: effect on invasive capacity of murine tumor cells and correlation with cathepsin (L + B) secretion. Clin Exp Metastasis 1997;15:19–25.
9. Sundfor K, Lyng H, Rofstad EK. Tumour hypoxia and vascular density as predictors of metastasis in squamous cell carcinoma of the uterine cervix. Br J Cancer 1998;78:822–7.
10. Höckel M, Schlenger K, Höckel S, Vaupel P. Hypoxic cervical cancers with low apoptotic index are highly aggressive. Cancer Res 1999;59:4525–8.
11. Walenta S, Wetterling M, Lehrke M, et al. High lactate levels predict likelihood of metastases, tumor recurrence, and restricted patient survival in human cervical cancers. Cancer Res 2000;60:916–21.
12. Ling C, Humm J, Larson S, et al. Towards multidimensional radiotherapy (MD-CRT): biological imaging and biological conformality. Int J Radiat Oncol Biol Phys 2000;47:551–60.
13. Peters KB, Brown JM. Tirapazamine: a hypoxia-activated topoisomerase II poison. Cancer Res 2002;62:5248–53.
14. Patterson A, Ferry D, Edmunds S, et al. Mechanism of action and preclinical antitumor activity of the novel hypoxia-activated DNA cross-linking agent PR-104. Clin Cancer Res 2007;13:3922–32.
15. Tan MH, Holyoke ED, Goldrosen MC. Murine colon adenocarcinomas: syngeneic orthotopic transplantation and subsequent hepatic metastases. J Natl Cancer Inst 1977;59:1537–44.
16. Fidler IJ, Naito S, Pathak S. Orthotopic implantation is essential for the selection, growth, and metastasis of human renal cell cancer in nude mice. Cancer Metastasis Rev 1990;9:149–65.
17. Kuo TH, Kubota T, Watanabe M, et al. Site-specific chemosensitivity of human small-cell lung carcinoma growing orthotopically compared to subcutaneously in SCID mice: the importance of orthotopic models to obtain relevant drug evaluation data. Anti Cancer Res 1993;13:627–30.
18. Hoffman RM. Orthotopic metastatic mouse models for anticancer drug discovery and evaluation: a bridge to the clinic. Invest New Drugs 1999;17:343–59.
19. Killion JJ, Radinsky R, Fidler IJ. Orthotopic models are necessary to predict therapy of transplantable tumors in mice. Cancer Metastasis Rev 1999;17:279–84.
20. Rosol TJ, Tannehill-Gregg SH, LeRoy BE, Mandl S, Contag CH. Animal models of bone metastasis. Cancer 2003;97:748–57.
21. Bibby MC. Orthotopic models of cancer for preclinical drug evaluation: advantages and disadvantages. Eur J Cancer 2004;40:852–7.
22. Cowen SE, Bibby MC, Double JA. Characterisation of the vasculature within a murine adenocarcinoma growing in different sites to evaluate the potential of vascular therapies. Acta Oncol 1995;34:357–60.
23. Greenberg NM, DeMayo F, Finegold MJ, et al. Prostate cancer in a transgenic mouse. Proc Natl Acad Sci U S A 1995;92:3439–43.
24. Jackson EL, Willis N, Mercer K, et al. Analysis of lung tumor initiation and progression using conditional expression of oncogenic K-ras. Genes Dev 2001;15:3243–8.
25. Arvanitis C, Felsher DW. Conditional transgenic models define how MYC initiates and maintains tumorigenesis. Semin Cancer Biol 2006;16:313–7.
26. Valenzuela DM, Groffen J. Four human carcinoma cell lines with novel mutations in position 12 of c-K-ras oncogene. Nucleic Acids Res 1986;14:843–52.
27. Tran PT, Fan AC, Bendapudi P, et al. Combined inactivation of MYC and K-ras oncogenes reverses tumorigenesis in lung adenocarcinomas and lymphomas. PLoS One 2008;3:e2125.
28. Reischl G, Ehrlichmann W, Bieg C, et al. Preparation of the hypoxia imaging PET tracer [18F]FAZA: reaction parameters and automation. Appl Radiat Isot 2005;62:897–901.
29. Graves EE, Quon A, Loo BW. RT_Image: an open-source tool for investigating PET in radiation oncology. Technol Cancer Res Treat 2007;6:111–21.
30. Raleigh JA, Chou SC, Arteel GE, Horsman MR. Comparisons among pimonidazole binding, oxygen electrode measurements, and radiation response in C3H mouse tumors. Radiat Res 1999;151:580–9.
31. Le Q, Chen E, Salim A, et al. An evaluation of tumor oxygenation and gene expression in patients with early stage non-small cell lung cancers. Clin Cancer Res 2006;12:1507–14.
32. Nordsmark M, Bentzen SM, Rudat V, et al. Prognostic value of tumor oxygenation in 397 head and neck tumors after primary radiation

therapy. An international multi-center study. Radiother Oncol 2005; 77:18–24.
33. Gross MW, Karbach U, Groebe K, Franko AJ, Mueller-Klieser W. Calibration of misonidazole labeling by simultaneous measurement of oxygen tension and labeling density in multicellular spheroids. Int J Cancer 1995;61:567–73.
34. Koch CJ, Evans SM, Lord EM. Oxygen dependence of cellular uptake of EF5 [2-(2-nitro-1H-imidazol-1-yl)-*N*-(2,2,3,3,3-pentafluoropropyl)a cet amide]: analysis of drug adducts by fluorescent antibodies vs bound radioactivity. Br J Cancer 1995;72:869–74.
35. Beck R, Roper B, Carlsen J, et al. Pretreatment 18F-FAZA PET predicts success of hypoxia-directed radiochemotherapy using tirapazamine. J Nucl Med 2007;48:973–80.
36. Rapisarda A, Uranchimeg B, Scudiero DA, et al. Identification of small molecule inhibitors of hypoxia-inducible factor 1 transcriptional activation pathway. Cancer Res 2002;62:4316–24.
37. Brown JM, Wilson WR. Exploiting tumor hypoxia in cancer treatment. Nat Rev Cancer 2004;4:437–47.
38. Timmerman R, Paulus R, Galvin J, et al. Stereotactic body radiation therapy for inoperable early stage lung cancer. J Am Med Assoc 2010;303:1070–6.
39. Chapman JD, Engelhardt EL, Stobbe CC, Schneider RF, Hanks GE. Measuring hypoxia and predicting tumor radioresistance with nuclear medicine assays. Radiother Oncol 1998;46:229–37.
40. Piert M, Machulla HJ, Picchio M, et al. Hypoxia-specific tumor imaging with 18F-fluoroazomycin arabinoside. J Nucl Med 2005; 46:106–13.
41. Busk M, Horsman M, Jakobsen S, et al. Imaging hypoxia in xenografted and murine tumors with 18F-fluoroazomycin arabinoside: a comparative study involving microPET, autoradiography, pO_2-polarography, and fluorescence microscopy. Int J Radiat Oncol Biol Phys 2008;70:1202–12.
42. Dehdashti F, Mintun MA, Lewis JS, et al. *In vivo* assessment of tumor hypoxia in lung cancer with 60Cu-ATSM. Eur J Nucl Med Mol Imaging 2003;30:844–50.
43. Eschmann S, Paulsen F, Reimold M, et al. Prognostic impact of hypoxia imaging with 18F-misonidazole PET in non-small cell lung cancer and head and neck cancer before radiotherapy. J Nucl Med 2005;46:253–60.
44. Li L, Yu J, Xing L, et al. Serial hypoxia imaging with 99mTc-HL91 SPECT to predict radiotherapy response in nonsmall cell lung cancer. Am J Clin Oncol 2006;29:628–33.
45. Spence A, Muzi M, Swanson K, et al. Regional hypoxia in glioblastoma multiforme quantified with [18F]fluoromisonidazole positron emission tomography before radiotherapy: correlation with time to progression and survival. Clin Cancer Res 2008;14:2623–30.
46. Brown JM. Tumor microenvironment and the response to anticancer therapy. Cancer Biol Ther 2002;1:453–8.
47. Rischin D, Hicks RJ, Fisher R, et al. Prognostic significance of [18F]-misonidazole positron emission tomography-detected tumor hypoxia in patients with advanced head and neck cancer randomly assigned to chemoradiation with or without tirapazamine: a substudy of Trans-Tasman Radiation Oncology Group Study 98.02. J Clin Oncol 2006;24:2098–104.